Three-dimensional Sparse Seismic Deconvolution based on Q Attenuation Model

Deborah Pereg and Israel Cohen, Technion – Israel Institute of Technology, and Anthony A. Vassiliou, GeoEnergy*

SUMMARY

We introduce a multichannel method to recover 3D reflectivity from 3D seismic data. The algorithm is formulated so that it promotes sparsity of the solution and also fits the earth Q-model of attenuation and dispersion propagation effects of reflected waves. In addition, the algorithm also takes into consideration spatial correlation between neighboring traces. These features, together with low computational cost, make the proposed method a good solution for the emerging need to process large volumes of 3D seismic data. The robustness of the proposed technique compared to single-channel recovery is demonstrated by synthetic and real data examples.

INTRODUCTION

Reflection Seismology aims at visualizing the internal structure of the subsurface. It enables detection of geological structures such as layers, traps and faults. When a short duration acoustic pulse (the wavelet) is transmitted into the ground, the reflected pulses are received by a sensor array placed on the ground, and further processed into 3D seismic data (Sherif and Geldart, 1983). Each seismic trace is described as a weighted superposition of one-dimensional (1D) pulses further degraded by additive noise, because the acoustic pulse is reflected at discontinuities in the medium impedance. The pulse is band-limited and changes over time. Our objectives are to recover the earth structure (the reflectivity) hidden in the observed seismic data, to increase its resolution and to overcome noise and attenuation of the reflected waves.

The seismic inversion problem is often solved by breaking the data into independent vertical 1D deconvolution problems. Each reflectivity channel is recovered from the corresponding inline trace or a cross line trace of a vertical cross section of the seismic data. The core assumptions are that a reflectivity channel is a sparse spike train, and that the wavelet is invariant in time and space (Berkhout, 1986; Ulrych, 1971; Wiggins, 1978; Taylor et al., 1979; Riel and Berkhout, 1985; Nguyen and Castagna, 2010; Zhang and Castagna, 2011; Gholami and Sacchi, 2012; Pham et al., 2014; Repetti et al., 2015).

Multichannel seismic deconvolution methods promote horizontal continuity of the seismic reflectivity by considering more than one trace in each channel estimation (Idier and Goussard, 1993; Mendel et al., 1981; Kormylo and Mendel, 1982; Kaaresen and Taxt, 1998; Heimer et al., 2007; Heimer and Cohen, 2009, 2008; Ram et al., 2010; Gholami and Sacchi, 2013; Mirel and Cohen, 2017; Pereg et al., 2017).

In (**?**) we presented a 1D algorithm that recovers the seismic reflectivity based on the earth Q-model. We also presented theoretical bounds on the recovery error, and on the localization error.

In this paper we summarizes some of the results in (Pereg et al., 2018). We present a new algorithm to recover 3D reflectivity signal from 3D seismic data. The problem is formulated so that the relations between spatially close traces are also taken into account using discontinuity measures (Cohen and Coifman, 2002; Cohen et al., 2006). The algorithm is applied to synthetic and real seismic data, demonstrating that the suggested method reveals reflectors amplitudes and locations with high precision.

SIGNAL MODEL

Reflectivity model

We assume an unknown 3D reflectivity signal. Each 1D channel (column) in the reflectivity is formulated as a superposition of point sources. In the discrete setting, assuming a sampling rate F_{s}, and that the set of delays $T = \{t_m\}$ lies on a grid $k/F_{\mathrm{s}},\ k \in \mathbb{Z}$, i.e., $k_m = t_m F_{\mathrm{s}}$, the reflectivity is given by

$$x[k] = \sum_m c_m \delta[k - k_m], \qquad k \in \mathbb{Z}, \qquad c_m \in \mathbb{R} \tag{1}$$

where $\delta[k]$ denotes the Kronecker delta function, $\sum_m |c_m| < \infty$, and $K = \{k_m\}$ is the set of discrete delays corresponding to the spikes locations. Each inline or crossline seismic discrete trace in the observed seismic 3D data is of the form

$$y[k] = \sum_n x[n] g_{\sigma,n}[k - n] + w[k], \qquad n \in \mathbb{Z} \tag{2}$$

where $\{g_{\sigma,n}\}$ is a known set of kernels corresponding to a possible set of time delays, $\sigma > 0$ is a known scaling parameter, and $w[k]$ is additive noise. In Pereg and Cohen (2017) we discuss specific requirements for $\{g_{\sigma,n}\}$. Our purpose is to reveal the true support $K = \{k_m\}$ and the spikes' amplitudes $\{c_m\}$ hidden in each of the seismic traces.

Note that the conventional convolution model assumes a time-invariant wavelet (Bendory et al., 2016b,a). Unfortunately, this assumption is often not satisfied. As in **?**, we suggest to take into consideration a set of different kernels $\{g_{\sigma,n}\}$. Each pulse in the set is determined according to the time (depth) t_n it corresponds to, in accordance with the earth Q model (**?**Wang, 2015, 2002; Kjartansson, 1979).

SEISMIC 3D RECOVERY

It is shown in **?** that single-channel recovery of the seismic reflectivity could be performed by solving the optimization problem

$$\min_{\hat{x} \in \ell_1(\mathbb{Z})} \|\hat{x}\|_1 \quad \text{subject to} \quad \|y[k] - \sum_n \hat{x}[n] g_{\sigma,n}[k - n]\|_1 \leq \delta, \tag{3}$$

where $\|\hat{x}\|_1 = \sum_k |\hat{x}[k]|$.

To this end, we consider 3D seismic data and develop a 3D recovery method based on convex optimization. We do not assume horizontal continuous layers or any other specific geological structure. Assume an inline or a crossline seismic trace $\mathbf{y}_{i,j}$ and $N-1$ spatially neighboring traces $\{\mathbf{y}_{i+u,j+v}\}$, where $(u,v)\in\Gamma$ such that $\Gamma\subseteq\{(u,v)\in\mathbb{Z}^2\ ,\ (u,v)\neq(0,0)\}$ and $|\Gamma|=N-1$. Denote some local discontinuity measure as a column vector $\mathbf{a}_{i,j}$. Each element $a_{i,j}[k]$ is associated with a distinguished point in some analysis cube, generically represented here by (i,j,k). We choose a measure such that $0\leq a_{i,j}[k]\leq 1$. For maximum discontinuity $a_{i,j}[k]=0$, whereas for minimum discontinuity $a_{i,j}[k]=1$. The value $a_{i,j}[k]$ describes the likelihood that a given point lies on a fault surface.

Assume G is an operator matrix such that $(G)_{k,n}=g_{\sigma,n}[k-n]$. Then, we can write

$$\mathbf{y}_{i,j}=G\mathbf{x}_{i,j}+\mathbf{w}_{i,j}, \tag{4}$$

where $\mathbf{x}_{i,j}$ is the corresponding reflectivity column and $\mathbf{w}_{i,j}$ is additive noise. Then, the estimated reflectivity column $\hat{\mathbf{x}}_{i,j}$ is the solution of the optimization problem

$$\begin{array}{ll}\min & \|\hat{\mathbf{x}}_{i,j}\|_1\\ \text{subject to} & f(\hat{\mathbf{x}}_{i,j})\leq\Delta,\end{array} \tag{5}$$

where

$$\begin{aligned}f(\hat{\mathbf{x}}_{i,j})=&\|\mathbf{y}_{i,j}-G\hat{\mathbf{x}}_{i,j}\|_2+\\ &\sum_{(u,v)\in\Gamma}\|A_{i,j}A_{i+u,j+v}(\mathbf{y}_{i+u,j+v}-G\hat{\mathbf{x}}_{i,j})\|_2,\end{aligned} \tag{6}$$

where $A_{i,j}=\mathrm{diag}(\mathbf{a}_{i,j})$, and $A_{i+u,j+v}=\mathrm{diag}(\mathbf{a}_{i+u,j+v})$. Since $A_{i,j}$ and $A_{i+u,j+v}$ describe the similarity between one spike (or null) location to close locations in a small volume, multiplying the residual error of neighboring traces by $A_{i,j}A_{i+u,j+v}$ enables the use of the available information about a group of channels, for the estimation of the true reflectivity value in each location in the volume. Wherever there is discontinuity in the volume, the estimation of this specific point does not rely on other close points.

Recovery-Error Bound for Horizontal Layers

Theorem 1 Assume N seismic traces that correspond to N identical reflectivity channels. Namely,

$$y_i[k]=\sum_n x[n]g_{\sigma,n}[k-n]+w_i[k],\ E\|w_i\|_2^2\leq\ S_{\mathrm{w}}^2,\ i=1,2...N, \tag{7}$$

where $\{g_{\sigma,n}\}$ is a set of admissible kernels sharing two common parameters $\varepsilon,\beta>0$ [see (Pereg and Cohen, 2017,Definition 2.1)] and E denotes mathematical expectation. In other words, the set $\{y_i\}_{i=1}^{i=N}$ consists of N smeared versions of N identical reflectivity columns, corrupted by N different noise realizations. We assume the support K is sufficiently separated, meaning that it obeys the minimal separation condition [see (Pereg and Cohen, 2017,Definition 2.2)], with a separation constant ν. Then, for $F_{\mathrm{s}}>0$, the solution $\hat{\mathbf{x}}$ of

$$\begin{array}{ll}\min & \|\hat{\mathbf{x}}\|_1\\ \text{subject to} & \sum_{i=1}^{N}\|\mathbf{y}_i-G\hat{\mathbf{x}}\|_2,\leq NS_{\mathrm{w}},\end{array} \tag{8}$$

satisfies

$$\|\hat{\mathbf{x}}-\mathbf{x}\|_2^2\leq\frac{64L_r\rho^2}{\beta^2\gamma_0^2}\frac{S_{\mathrm{w}}^2}{N}. \tag{9}$$

where L_r is the length of the estimated signal,

$$\rho\ \triangleq\max\left\{\frac{\gamma_0}{\varepsilon^2},(F_{\mathrm{s}}\sigma)^2\alpha_0\right\}$$

$$\alpha_0=\max_n g_{\sigma,n}(0),\quad \gamma_0=\min_n g_{\sigma,n}(0).$$

This bound ensures that given N traces, under the separation condition, a signal of the form (2), can be recovered by solving the optimization problem formulated in (8). A detailed proof is given in Pereg et al. (2018) for the precise recovery of the reflectivity spikes temporal locations, and the precise amplitudes recovery of the reflectivity spikes.

The bound in (9) guarantees that the mean squared error of the recovery is bounded. The error depends on the noise level and on the attenuation of the reflected waves. Most importantly the theoretical bound, affirmed by experimental results, demonstrates that given N realizations of the same reflectivity channel (as we have for horizontal reflectors), we can reduce the noise power by at least a factor of N. In the noise-free case where $S_{\mathrm{w}}=0$, whether the spikes amplitudes are small or large, the restoration of the reflectivity is exact.

In the time-variant setting most cases comply with $\gamma_0/\varepsilon^2<(F_{\mathrm{s}}\sigma)^2\alpha_0$. Then, the recovery error is bounded by

$$\|\hat{\mathbf{x}}-\mathbf{x}\|_2^2\leq 64\frac{L_r(F_{\mathrm{s}}\sigma)^4}{\beta^2}\left(\frac{\alpha_0}{\gamma_0}\right)^2\frac{S_{\mathrm{w}}^2}{N}.$$

The error is linear with respect to the noise level S_{w}^2 and inversely proportional to the number of channels, N. Moreover, the bound verifies that the error increases as Q gets smaller because small Q values correspond to higher α_0/γ_0 ratios and smaller β values. In addition, since β measures the flatness of the kernel near the origin, we can see that flat kernels result in more false detections.

EXPERIMENTAL RESULTS

Synthetic Data

We constructed a synthetic data set, simulating 2D reflectivity with two apparent faults. The reflectivity depicted in Fig. 1(a) consists of 30 traces, each of 128 samples, with sampling interval of $T_{\mathrm{s}}=4$ms. We created the seismic data as described in (2) using the Q-model, with Q=200. The initial wavelet was a Ricker wavelet with $\omega_0=50\pi$, i.e., 25Hz. To further degrade the signal and evaluate the recovery in noisy environment we added white Gaussian noise. The SNR is 5dB. The seismic data is shown in Fig. 1(b). The estimated reflectivities, obtained by single-channel and by the proposed multichannel recovery method are shown in Fig. 2. In this example, we set $N=3$. The optimization is performed by considering each reflectivity column and both the preceding and subsequent reflectivity columns. As a measure of discontinuity we use a binary version of Local Structural Entropy (LSE) (Cohen and Coifman, 2002). The correlation coefficient, between

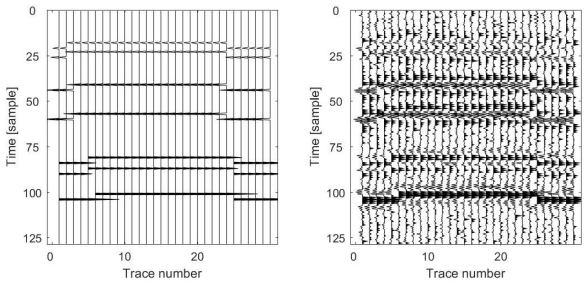

(a) (b)

Figure 1: Synthetic reflectivity and seismic data: (a) Synthetic 2D reflectivity section; (b) 2D seismic data (SNR = 5 dB).

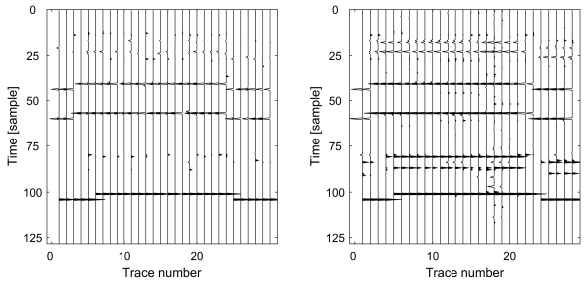

(a) (b)

Figure 2: Synthetic 2D recovery results: (a) Single-channel; (b) Multichannel.

the original reflectivity and the estimated reflectivity, achieved by single-channel deconvolution is $\rho = 0.86$. The correlation coefficient with the multichannel method, is $\rho = 0.95$. Visually comparing the results, it can be seen that the multichannel solution is more accurate. The single-channel solution fails to recover parts of the layer boundaries.

Figure 3 presents one example of the recovery error $\|\hat{x} - x\|_2^2$ as a function of the number of traces $1 \leq N \leq 30$ for $Q = 500$ and SNR = 5dB, $T_s = 4$ ms and $L_r = 176$. As in Fig. 1, the reflectivity is modeled as a zero-mean Bernoulli-Gaussian process. The minimum distance between two spikes satisfies the minimal separation condition. The initial wavelet was a Ricker wavelet with $\omega_0 = 100\pi$, i.e., 50Hz. As can be seen in Fig. 3 the error is inversely proportional to the number of traces, according to what we derived in Theorem 1.

Real Data

We applied the proposed method, to real seismic data from a small land 3D survey in the Gulf of Mexico (courtesy of GeoEnergy Inc., TX). The time interval is 4ms, inline trace spacing is 25m, and crossline trace spacing is 50m. A small subvolume with an inline distance of 5.025 km and a crossline distance of 10.05 km (201×201 traces) is used for demonstration. Each trace is 1.808 sec in duration (452 samples). The corresponding cross-section through the LSE volume, obtained with analysis cubes of size [2 2 14] is displayed in Figure 4(b). Figure 4(a) shows a vertical cross-section at $x = 2.5$ km through the seismic data. Assuming an initial

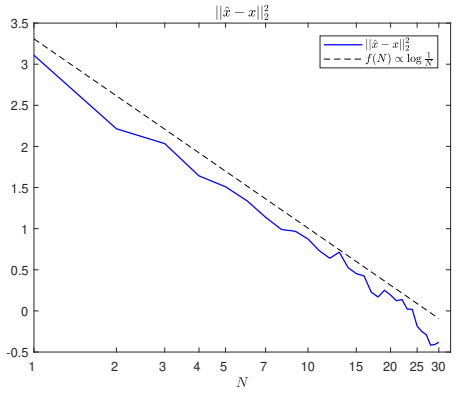

Figure 3: Recovery error $\log(\|\hat{x} - x\|_2^2)$ as a function of the number of traces N for $Q = 500$.

Ricker wavelet with $\omega_0 = 50\pi$ (25Hz), we estimated $Q = 233$ as described in Zhang and Ulrych (2002). A cross-section of the single-channel recovered reflectivity section is shown in Fig. 5(a). Each reflectivity column is recovered by taking into consideration two neighboring traces - one in the same vertical cross section and one in the adjacent cross section.

Visually examining these reflectivity sections, it can be seen that the layer boundaries in the estimates are distinct. Both structural and stratigraphic features can be observed in the images. Also, the reconstructed seismic data fits to the original given observation. We measure the accuracy in the location and amplitude of the recovered reflectivity spikes by the correlation coefficient between the reconstructed data to the given seismic data. In this example we have $\rho_{y,\hat{y}} = 0.81$ for the multichannel result. For single-channel recovery we have $\rho_{y,\hat{y}} = 0.78$.

Another example is presented in Figs. 6 and 7. Here we used a subvolume of 401×401 traces. Each trace is 1001 samples long. The time interval is 4 ms; inline and cross line trace spacing is 25 m. Figure 6(a) shows a vertical cross section through the seismic data. As a measure of discontinuity we used the skeletonized local-fault-extraction (LFE) (Cohen et al., 2006). The seismic data through the LFE is presented in Fig. 6(b). Assuming an initial Ricker wavelet with $\omega_0 = 50\pi$ (25Hz), we estimated $Q = 200$. A cross-section of the recovered reflectivity section by single-channel method is shown in Fig. 7(a). Figure 7(b) shows the recovered reflectivity cross-section of a 3-channel implementation (i.e., $N = 3$), taking into consideration two neighboring traces - one in the same vertical cross section and one in the adjacent cross section. Here, we have $\rho_{y,\hat{y}} = 0.90$ for the multichannel result, and for the single-channel recovery we have $\rho_{y,\hat{y}} = 0.88$.

CONCLUSIONS

We presented a 3D adaptive seismic recovery algorithm based on a time-variant model. The algorithm promotes sparsity of the solution and also considers attenuation and dispersion effects. The recovery takes into account the relations between

neighboring traces in the 3D volume. The algorithm is suitable for large volumes of data. We demonstrated its performance with synthetic and real data in highly attenuating noisy environment.

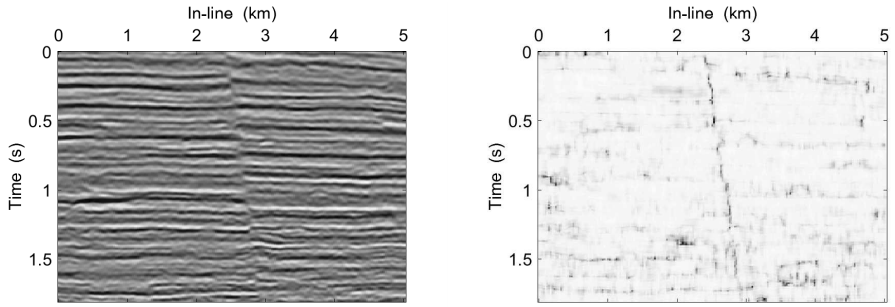

(a) (b)

Figure 4: Vertical cross-section at $x = 2.5$km through: (a) seismic data; (b) LSE volume of size $[2\ 2\ 14]$.

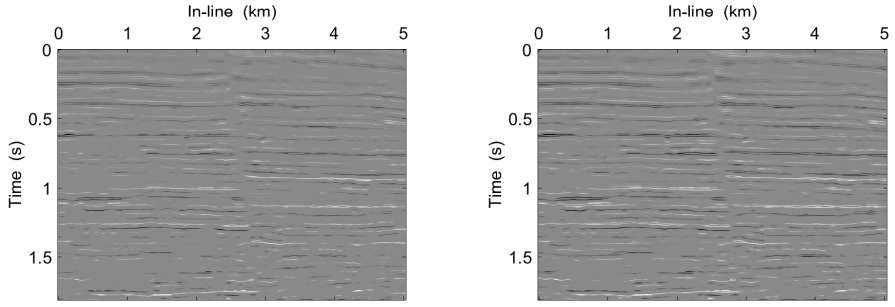

(a) (b)

Figure 5: Real data inversion results: (a) Estimated reflectivity - single-channel; (b) Estimated reflectivity - multichannel.

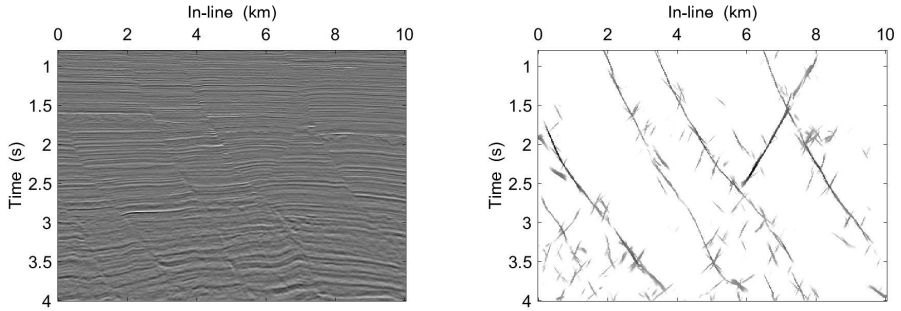

(a) (b)

Figure 6: Vertical cross-section at $y = 1.3$km through: (a) seismic data; (b) skeletonized LFE volume.

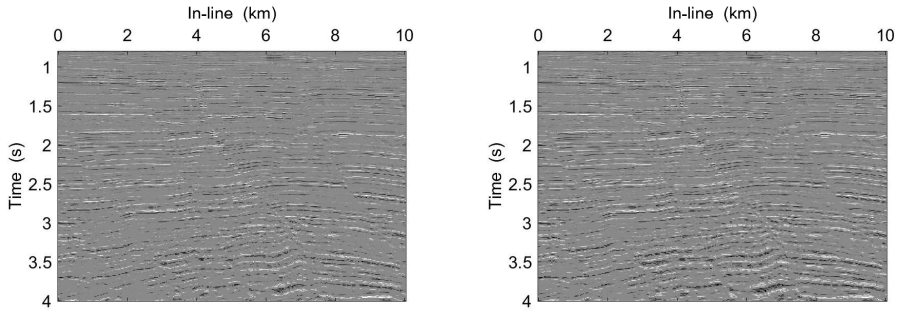

(a) (b)

Figure 7: Real data inversion results: (a) Estimated reflectivity - single-channel; (b) Estimated reflectivity - multichannel.

REFERENCES

Bendory, T., S. D. A. Bar-Zion, and A. Feuer, 2016a, Stable support recovery of stream of pulses with application to ultrasound imaging: IEEE Transaction on Signal Processing, **64**, 3750 – 3759.

Bendory, T., S. Dekel, and A. Feuer, 2016b, Robust recovery of stream of pulses using convex optimization: Journal of mathematical analysis and applications, **442**, 511–536.

Berkhout, A., 1986, The seismic method in the search for oil and gas: current techniques and future development: proceedings of the IEEE, **74**, 1133–1159.

Cohen, I., and R. Coifman, 2002, Local discontinuity measures for 3D seismic data: Geophysics, **67**, 1933–1945.

Cohen, I., N. Coult, and A.A.Vassiliou, 2006, Detection and extraction of fault surfaces in 3D seismic data: Geophysics, **71**, P21–P27.

Gholami, A., and M. D. Sacchi, 2012, A fast and automatic sparse deconvolution in the presence of outliers: IEEE Trans. Geosci. Remote Sens., **50**, 4105–4116.

———, 2013, Fast 3D blind seismic deconvolution via constrained total variation and GCV: SIAM J. Imaging Sci, **6**, 2350–2369.

Heimer, A., and I. Cohen, 2008, Multichannel blind seismic deconvolution using dynamic programmming: Signal Processing, **88**, 1839–1851.

———, 2009, Multichannel seismic deconvolution using Markov-Bernoulli Random Field modeling: IEEE Trans. Geoscience and Remote Sensing, **47**, 2047–2058.

Heimer, A., I. Cohen, and A. Vassiliou, 2007, Dynamic programming for multichannel blind seismic deconvolution: Proc. Society of Exploration Geophysicist International Conference, Exposition and 77th Annual Meeting, 1845–1849.

Idier, J., and Y. Goussard, 1993, Multichannel seismic deconvolution: IEEE Trans. Geoscience, Remote sensing, **31**, 961–979.

Kaaresen, K., and T. Taxt, 1998, Multichannel blind deconvolution of seismic signals: Geophysics, **63**, 2093–2107.

Kjartansson, E., 1979, Constant Q-wave propagtion and attenuation: Journal of Geophysical Research, 4737–4747.

Kormylo, J., and J. Mendel, 1982, Maximum likelihood detection and estimation of Bernoulli-Gaussian processes: IEEE Trans. Information Theory, **28**, 482–488.

Mendel, J., J. Kormylo, F. Aminzadeh, J. Lee, and F.Habibi-Ashrafi, 1981, A novel approach to seismic signal processing and modeling: Geophysics, **46**, 1398–1414.

Mirel, M., and I. Cohen, 2017, Multichannel semi-blind deconvolution of seismic signals: Signal Processing, **135**, 253–262.

Nguyen, T., and J. Castagna, 2010, High resolution seismic reflectivity inversion: Journal of Seismic Exploration, **19**, 303–320.

Pereg, D., and I. Cohen, 2017, Seismic signal recovery based on earth Q model: Signal Processing, **137**, 373 – 386.

Pereg, D., I. Cohen, and A. Vassiliou, 2018, Seismic 3D: submitted to Signal Processing.

Pereg, D., I. Cohen, and A. A. Vassiliou, 2017, Multichannel sparse spike inversion: Journal of Geophysics and Engineering, **14**, 1290.

Pham, M. Q., L. Duval, C. Chaux, and J.-C. Pesquet, 2014, A primal-dual proximal algorithm for sparse template-based adaptive filtering: Application to seismic multiple removal: IEEE Trans. Signal Process., **62**, 4256–4269.

Ram, I., I.Cohen, and S. Raz, 2010, Multichannel deconvolution of seismic signals using statistical MCMC methods: IEEE Trans. Signal Processing, **58**, 2757–2769.

Repetti, A., M. Q. Pham, L. Duva, E. Chouzenoux, and J.-C. Pesquet., 2015, Euclid in taxicab: sparse blind deconvolution with smoothed ℓ_1/ℓ_2 regularization: IEEE Signal Processing Letters, **22**, 539–543.

Riel, P. V., and A. J. Berkhout, 1985, Resolution in seismic trace inversion by parameter estimation: Geophysics, **50**, 1440–1455.

Sherif, R., and L. Geldart, 1983, Exploration seismology, 2 ed.: Cambridge University Press.

Taylor, H. L., S. C. Banks, and J. F. McCoy, 1979, Deconvolution with the ℓ_1 norm: Geophysics, **44**, 39–52.

Ulrych, T., 1971, Application of homomorphic deconvolution to seismology: Geophysics, **36**, 650–660.

Wang, Y., 2002, A stable and efficient approoach of inverse Q filtering: Geophysics, **67**, 657–663.

———, 2015, Frequencies of the Ricker wavelet: Geophysics, **80**, A31–A37.

Wiggins, R., 1978, Minimum entropy deconvolution: Geoexploration, **16**, 21–35.

Zhang, C., and T. Ulrych, 2002, Estimation of quality factors from CMP record: Geophysics, **67**, 1542–1547.

Zhang, R., and J. Castagna, 2011, Seismic sparse-layer reflectivity inversion using basis pursuit decomposition: Geophysics, **76**, 147–158.